Journal of Modern Physics, 2011, 2, 1178-1186
doi:10.4236/jmp.2011.210147 Published Online October 2011 (http://www.SciRP.org/journal/jmp)

Structural and Optical Dispersion Characterisation of Sprayed Nickel Oxide Thin Films

Safwat A. Mahmoud[1*], Shereen Alshomer[1,2], Mou'ad A. Tarawnh[3]
[1]*Physics Department*, *Faculty of Science*, *University of Hail*, *Hail*, *Kingdom of Saudi Arabia*
[2]*The National University of Malaysia*, *Bangi*, *Malaysia*
[3]*School of Applied Physics*, *Faculty of Science and Technology*, *The National University of Malaysia*, *Banji*, *Malaysia*
E-mail: *samahmoud2002@yahoo.com
Received January 24, 2011; *revised June* 10, 2011; *accepted June* 23, 2011

Abstract

Crystalline and non-crystalline nickel oxide (NiO) thin films were obtained by spray pyrolysis technique (SPT) using nickel acetate tetrahydrate solutions onto glass substrates at different temperatures from 225 to 350˚C. Structure of the as-deposited NiO thin films have been examined by X-ray diffraction (XRD) and atomic force microscope (AFM). The results showed that an amorphous structure of the films at low substrate temperature (T_s = 225˚C), while at higher $T_s \geq 275$˚C, a cubic single phase structure of NiO film is formed. The refractive index (n) and the extinction coefficient (k) have been calculated from the corrected transmittance and reflectance measurements over the spectral range from 250 to 2400 nm. Some of the optical absorption parameters, such as optical dispersion energies, E_o and E_d, dielectric constant, ε, the average values of oscillator strength, S_o, wavelength of single oscillator λ_o and plasma frequency, ω_p, have been evaluated.

Keywords: Nickel Oxide Thin Films, Nickel Acetate, Optical Dispersion, Spray Pyrolysis Technique, AFM, XRD

1. Introduction

The optical properties of thin films are very important for many applications, including interference devices, such as antireflection coatings, laser mirrors and monochromatic filters, as well as optoelectronics, integrated optics, solar power engineering, microelectronics and optical sensor technology depending on the reflectance and transmittance properties of the films during their preparation.

Dispersion models parameterize the spectral dependencies on the dielectric functions of films or corresponding functions, such the band gap, optical dispersion energies, E_o, E_d, dielectric constant, ε, ratio between the number of charge carriers and the effective mass, N/m^*, wavelength of the single oscillator, λ_o, plasma frequency…etc., can be determined by data treatment. The optical constants of thin films provide us with information concerning with microscopic characteristics of the material.

Transition metal oxides like nickel oxides have found wide applications due to these anti-ferromagnetic semiconductor with wide gab ≈ 3.6 eV and cubic rock salt-like crystal structure [1,2]. It offers promising candidature for many application such as electrocatalysis [3], positive electrode in batteries [4], fuel cell [5], electrochromic devices [6], solar thermal absorber [7], catalyst for oxygen evolution [8] and photo electrolysis [9]. Several physical and chemical methods, such as sputtering [10], pulsed laser deposition [11], chemical bath deposition [10,12] and sol-gel [13] have been used to obtain nickel oxide films. All these methods offer different advantages depending on the application of interest and many efforts have been conduced to obtain films with the desirable physical and/or chemical properties. Among the different methods for film deposition, the relative simplicity of the spray pyrolysis method and its potential application for large area deposition make it very attractive, low cost and feasible for mass production processes.

This paper reports the influence of substrate temperature (T_s) as an important parameter on the preparation of nickel oxide (NiO) thin films by spray pyrolysis tech-

nique (SPT) using nickel acetate tetrahydrate solutions onto glass substrates. The accurate determination of the optical constants of these materials is important, not only in order to know the basic mechanisms underlying these phenomena, but also to exploit and develop their interesting technological applications. Therefore, the optical absorption parameters, such as optical dispersion energies, E_o, and E_d, dielectric constant, ε, the average values of oscillator strength S_o, wavelength of single oscillator λ_o, and plasma frequency, ω_p, have been evaluated under the effect of substrate temperature.

2. Experimental Details

2.1. Film Preparation

Nickel acetate tetrahydrate ($Ni(C_2H_3O_2)_2{\cdot}4H_2O$) in a concentration of 5×10^{-2} M in ethanol was used as a starting solution for deposition of nickel oxide films. Nickel acetate tetrahydrate decomposes in a two step-process, firstly dehydration from 95˚C to 150˚C and secondly decomposition of the acetate between 300˚C to 350˚C [14,15]. The solution was passed through a pneumatic nebulizer with a nozzle diameter of 0.7 mm. The spraying process lasted for about 15 s. The period between spraying processes was about 3 min; this period is enough to avoid excessive cooling of glass substrate. The overall reaction process can be expressed as heat decomposition of nickel acetate to clusters of nickel oxide in the presence of water and air oxygen.

In order to explore the influence of the ultrasonically cleaned preheated glass substrate temperature (Ts), different deposition temperatures ranged between 225 to 350˚C were used to prepare these films. In order to get uniform thin films, the height of spraying nozzle, solution molarity and the rate of spray process were kept constant during the deposition process at 35 cm, 5×10^{-2} M and 15 cm^3/min, respectively. A thermocouple was fixed to the substrate surface using silver past and the temperature was measured at the four corners of the glass substrate surface, then the results were averaged and the standard deviation was calculated (± 5˚C).

2.2. Thickness Measurements

Thickness of the as-deposited films prepared at different substrate temperatures was determined by multiple-beam Fizeau fringes at reflection using either white light or monochromatic light (Hg, λg = 546 nm). A glass substrate was partially masked during deposition of the film to obtain a sharp edge. Then, a thermally evaporated aluminum layer coated the total surface of the substrate. The colored interference fringes enabled the determination of the order of magnitude of the fringes shift, while the monochromatic fringe shift, as a fraction of the order separation was measured using an eyepiece micrometer.

2.3. Structural Investigation

Crystallinity and the phases of the as-deposited films were characterized using JEOL X-ray diffractometer (XRD) (Model JSDX-60PA) with monochromatic high-intensity Cu K_α radiation (λ = 0.154184 nm). Continuous scanning was applied with a slow scanning speed (1˚/min) and a small time constant (1 s).

2.4. Microstructure Analysis

Atomic force microscope (AFM) was used to analyze microstructures by molecular imaging in two- and three-dimensions. The atomic cross-section and surface roughness were determined. Each sample before AFM investigation was washed carefully with distilled water and dried. A Nanoscope III instrument with a 100 μm long silicon tip with repulsive and constant interaction force less than a few nano-Newtons were used [16].

2.5. Optical Measurements

Optical transmission and reflection of the prepared films were recorded over the wavelength range from 250 - 2400 nm using Shimadzu UV 3101 PC; UV-Vis-NIR double-beam spectrophotometer with reflection attachment based on V-N geometry (incident angle 5˚). The spectral variation of transmission and reflection obtained in this work are used to provide a qualitative guide to the film quality. A laboratory developed computer program [16] was used to calculate the absorption coefficient, energy gaps, optical constants and dielectric constants.

3. Results and discussion

3.1. Variation of the Film Thicknesses with Substrate Temperature

Thickness of the obtained films was investigated as a function of the substrate temperatures ranged between 225˚C and 350˚C and the data are graphically represented in **Figure 1**. It was found that the film thickness decreases with increasing the substrate temperature despite the fact that, the kinetics of the NiO forming reaction should increase with temperature. The observed dependence can be explained by the diminished mass transport to the substrate at higher temperature due to gas convection from bath pushing the droplets of the precursor, as well as the rate of re-evaporation was increased at

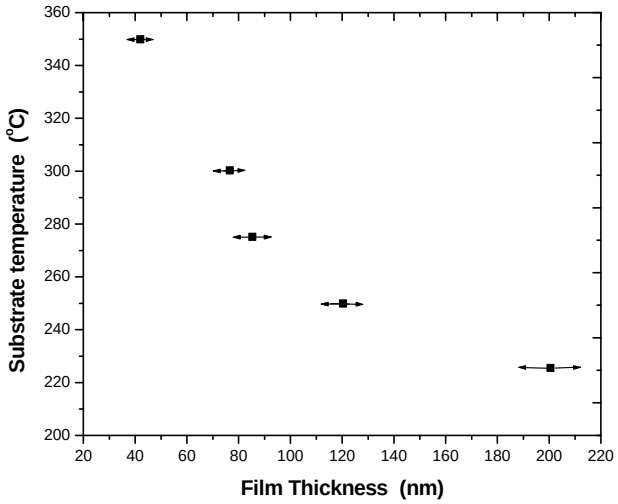

Figure 1. Variation of film thicknesses with substrate temperatures.

higher temperatures. In addition, the decrease in the film thickness may be attributed to water loss [17] or removal of interlayer water with consequent formation of compact NiO films.

3.2. Structural Characterization

Figure 2 shows the variation of the diffraction patterns as a function of the substrate temperature. The Bragg geometry is employed for analysis and the results of XRD for the as-deposited NiO films at T_s = 225˚C – 250˚C show that the film structure is non-crystalline structure. Further increasing in the substrate temperature up to ≥ 275˚C, the films were fully transformed to polycrystalline phase of NiO (JCPDS 47-1049) with cubic structural [9,18,19].

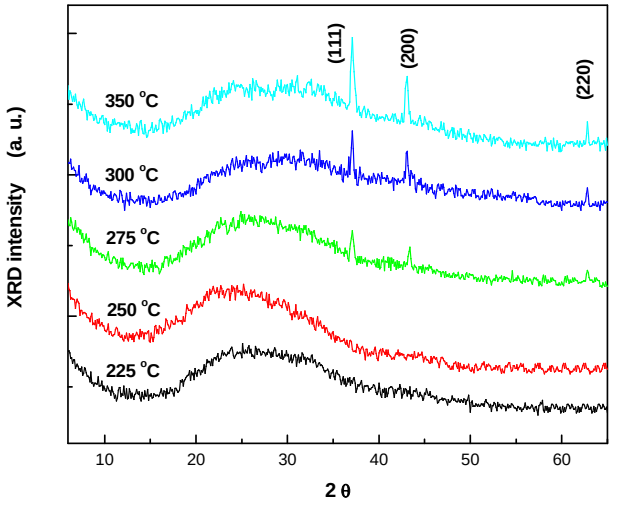

Figure 2. The X-ray diffractograms of NiO films at different substrate temperatures.

Three peaks are observed in the pattern at 2θ = 37.1˚, 43.3˚ and 62.8˚ assigned to the (111), (200) and (220) crystal planes, respectively. The estimated lattice parameters was found to be a = b = c = 0.417 nm. The increase in the amount and degree of crystallinity of the phase is indicated by the enhancement of the peak intensity. Furthermore, no other peaks corresponding to other phases have emerged. This suggested that, NiO phase is stable and its formation is independent of substrate temperature. The films show prefential growth along the [111] direction. The increase in the intensity of the peaks may be attributed to the increase in the degree of crystallinity caused by increasing the substrate temperature.

Scherre's formula on the bases of full-wave at Half-Maximum (FWHM) was used to calculate the grain size and the average grain size was found to increase from 38 to 45 nm with increasing the substrate temperature from 275˚C to 350˚C.

3.3. Microstructural Characterization

Figure 3 shows a NiO crystal surface imaged with the AFM in air and the three-dimensional plot (**Figure 3(a)**) atomic corrugations are visible as well as grains can be seen on the thin film (**Figure 3(b)**). The relative smooth surface could be seen with 45 nm thick. A grain size analysis of the thicker NiO film gives a mean grain size area of 3.9 μm^2. This means that an average radius of the grains of ≈ 35 nm could be determined. These data are found to be in a good agreement with XRD measurements.

The roughness analysis and the cross section profile shown in **Figure 3(c)** give an impressive insight of the excellent capability of the method to measure surface topography. The surface roughness, (R) is the mean roughness of the surface relative to the center plane of the glass substrate ranged between 0.5 and 1.5 nm. However, the thicker film was found to have a greater roughness than that of the thinner one.

3.4. Optical Characterization

Optical measurements of transmittance and reflectance of the films deposited at different substrate temperatures are shown in **Figure 4**. These measurements have been taken in the wavelength range from 250 to 2400 nm. The optical properties of the investigated films were studied by the method of the spectral optical absorption and reflection. The spectral data of normal transmittance, $T_{exp}(\lambda)$, and reflectance, $R_{exp}(\lambda)$, were corrected due to substrate effect according to the following formula [20].

$$T(\lambda) = \frac{T_{exp}T_{sub}\left(1 - R_{exp}R_{sub}\right)}{T_{sub}^2 - T_{exp}^2 R_{exp}^2} \quad (1)$$

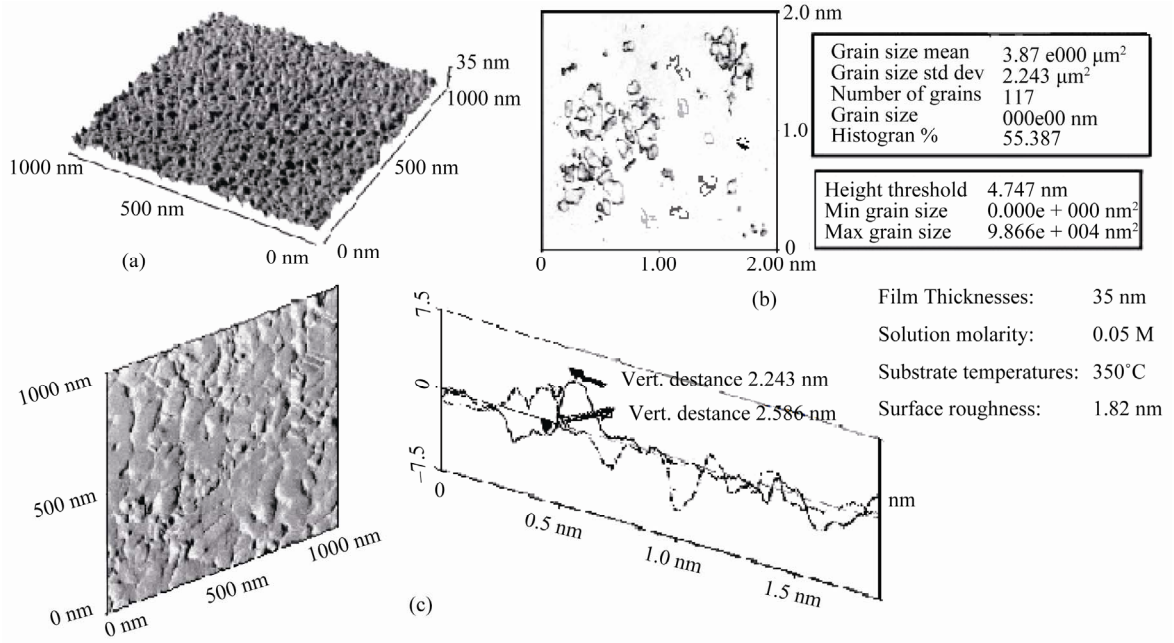

Figure 3. Three-dimensional AFM images of atomic resolution of NiO films (a), AFM images with total number of grains, mean and standerd deviation of of defined grains (b), with corresponding atomic cross-section analysis of NiO thin films (c).

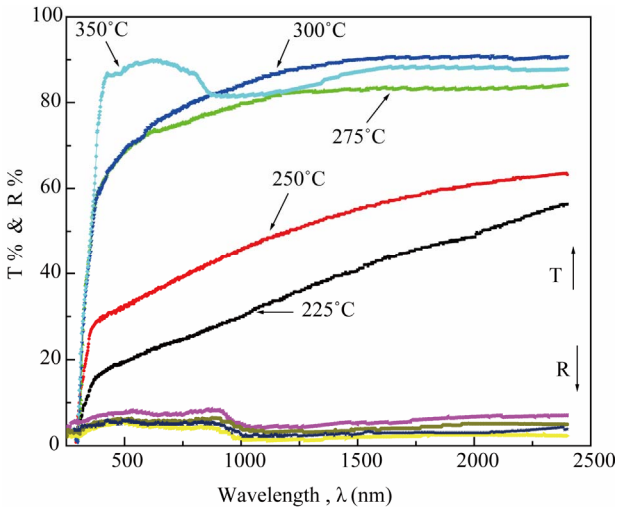

Figure 4. The transmittance spectrum of NiO films prepared at different substrate temperature.

$$R(\lambda) = \frac{R_{exp}T_{sub}^2 - T_{exp}^2 R_{sub}}{T_{sub}^2 - T_{exp}^2 R_{sub}^2} \qquad (2)$$

where T_{sub} and R_{sub} are the transmittance and the reflectance of the glass substrate respectively. As shown in **Figure 4**, the general increase in the transmittance is observed as the film thickness decrease. This behavior may be attributed to perfection and stoichiometry of the films.

Anomalous behaviour is observed at low substrate temperature that disappearing in the absorption edge and lowering in the transmittance. This probably is due to the following reasons.

1) Transformation of the phase from amorphous to crystalline considering the sample prepared at $T_s = 250$˚C as a critical case.

2) Absorption edge disappeared in the films that deposited in low temperature; this is due to the fact that, as Ts decreases, bigger clusters are formed before the film creation and the scattered radiation became remarkable due to the surface roughness.

3) Adsorption of water in films deposited at low temperatures during the handling of the film.

3.4.1. Optical Energy Gap

From the transmittance data and according to Tauc [21] relation, $(\alpha E)^2$ versus incident photon energy, (E), plots were obtained. The graphs are represented in **Figure 5**. The band gap energy values are found to be 3.83 and 3.14 eV for the NiO thin films with increasing the substrate temperature from 225˚C to 350˚C, which are in a good agreement with that obtained for normal bulk NiO (3.6 - 4.0 eV) [22].

Furthermore, it is well known that the energy gap of the semiconductor increases with the decrease of the grain size. NiO nanotubes embedded in porous anodic alumina template also demonstrated a strong absorption in the UV region and showed a band gap of 3.9 eV which is quite close to our result [23]. The decrease in E_g with T_s can be attributed to crystallinity improvement of films deposited at high substrate temperatures.

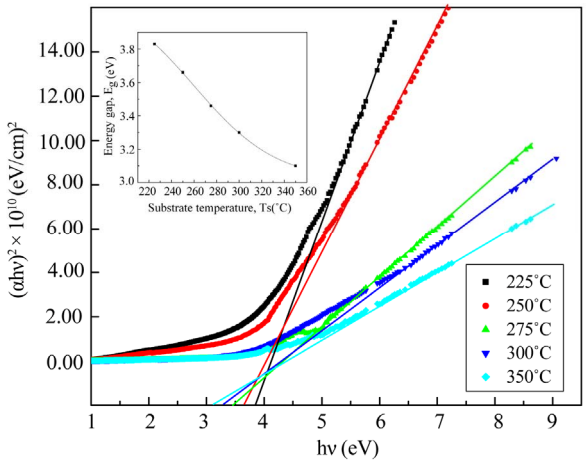

Figure 5. The $(\alpha h\nu)^2$ vs. hν plot for NiO thin films at different substrate temperature.

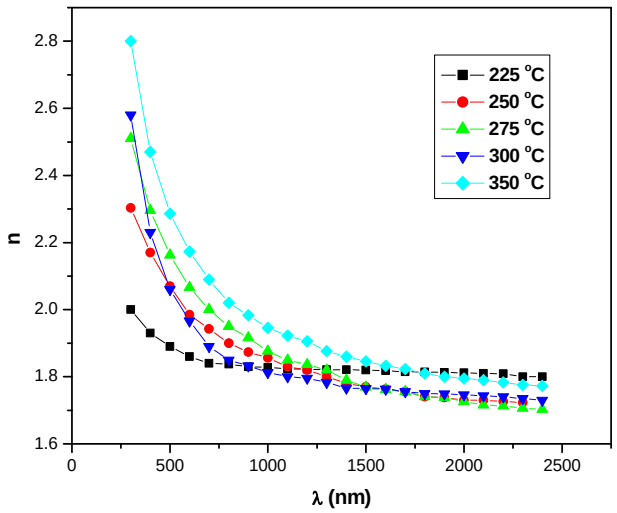

Figure 6. The refractive index (n) of NiO films as a function of wavelength λ, at different substrate temperatures.

3.4.2. Determination of Refractive Index

Refractive index is one of the fundamental properties for an optical material because it is closely related to the electronic polarization of ions and the local field inside materials. The complex optical constant (refractive index, (n)) of the prepared samples has been calculated from the corrected $T(\lambda)$ and $R(\lambda)$ using a developed computation program [24].

$$R(\lambda) = \frac{(n-1)^2}{(n+1)^2}$$

and

$$T(\lambda) = \frac{4n}{(n+1)^2} \qquad (3)$$

where n is the refractive index of the thin film. The reflectance, R, at the vacuum-film interface has to take into consideration with the value of extinction coefficient, k, so that R can be written as Karmers-Kronig relation.

$$R = \left[\frac{(n-1)^2 + k^2}{(n+1)^2 + k^2}\right] \qquad (4)$$

The behaviour of refractive index has a higher value at very low wavelength (strong absorption). This is due to the quality between the frequency of incident electromagnetic radiation and the plasma frequency. Therefore, there is an anomalous dispersion of refractive index in the region of the plasma frequency. But when λ crosses λ_p (plasma wavelength) and the corresponding dielectric constant becomes negative, the refractive index becomes largely imaginary. Hence, there is no propagation of electromagnetic radiation through the medium and gets reflection as mentioned before.

Figure 6 shows the spectral variation of the refractive index as a function of wavelength at different substrate temperatures. It can be seen that, the maximum value of refractive index (n = 2.8 at T_s = 350˚C) at very low wavelength, λ = 300 nm (strong-absorption region), was observed in all samples. This is due to the equality between the frequency of incident electromagnetic radiation and the frequency of electrons. This leads to the coupling of electrons in NiO films to the oscillating electric field. At longer wavelengths, λ > 500 nm, the refractive index is sharply decreasing for all patterns reaching to the lowest value of 1.8 at $\lambda \geq$ 900 nm and then the n value remains slightly changed for the whole wavelength. Furthermore, the behaviors of refractive index of all films are similar, which is due to the normal dispersion. In the NIR region, $\lambda \geq$ 1000 nm, the n values differ slightly with substrate temperature, which diverge remarkably in the visible region. These results are in good agreement with the data obtained by others [9] in the same phase.

3.4.3. Determination of Dielectric Constant

Analyses of the obtained data of refractive index can be used to obtain the high frequency dielectric constant through two procedures [25]: The first, describes the contribution of the free carriers and lattice vibration modes of the dispersion, while the second procedure is based upon the dispersion arising from the bound carriers in an empty lattice. However, both procedures were employed for the obtained value of lattice high frequency dielectric constant ε_∞.

3.4.3.1. The First Procedure

The following equation shows the relation between the optical dielectric constant ε, wavelength λ and refractive

index [26]:

$$\varepsilon = n^2 = \varepsilon_{\infty(1)} - \left(\frac{e^2}{4\pi c^2 \varepsilon_o}\right)\left(\frac{N}{m^*}\right)\lambda^2 \quad (5)$$

where c is the velocity of the light, ε_o the permittivity of free space (8.854×10^{-12} F/m), N the free carrier concentration and m^* the effective mass of the charge carriers. The nature of the dispersion of n^2 as a function of wavelength (λ^2) for different substrate temperatures is shown in **Figure 7**. As shown un this Figure, the refractive index is an anomalous dispersion in the region of the high frequency. Both the refractive index and increases and absorption of electromagnetic radiation were found to be increased as frequency increases. Furthermore, the refractive index becomes largely, when the frequency of the radiation crosses with the characteristic frequency of the electron. Hence, there is no propagation of electromagnetic radiation through the NiO films. From **Figure 7**, it can be seen that the dependence of n^2 is linear at longer wavelength. The values of lattice high frequency dielectric constant, $\varepsilon_{\infty(1)}$, is determined from the intersection of the straight line with $\lambda^2 = 0$. The values of $\varepsilon_{\infty(1)}$ increased with increasing substrate temperature (subfigure). **Table 1** shows the values of both $\varepsilon_{\infty(1)}$ and the ratio, N/m^*, of the investigated films at different substrate temperatures, which determined from the intercept and slopes of the line, respectively. The obtained values of the ration N/m^* were in the range between 6.25×10^{40} to 5.49×10^{40} $cm^{-3} \cdot g^{-1}$ with different substrate temperatures. These results are in a good agreement with Al-Ghamdi *et al.* [19] for NiO thin films and Hutchines *et al.* [27] and El-Nahass *et al.* [28] found (N/m^*) for WO_3, nickel phthalocyanine films, and also for $TiInS_2$ single crystal [29], in the same order. It is known that in the range of transparency, when the electron damping parameter $\gamma \ll \omega$,

$$n^2 = \varepsilon_\infty - \frac{\omega_p^2}{\omega^2} n^2 \quad (6)$$

where ω_p is the plasma frequency and $\omega_p^2 = e^2 N / \varepsilon_o m^*$, and ω the incident light frequency [30,31]. From the approximation of the linear part of the dependences $n^2(\lambda^2)$ of NiO films deposited at different substrate temperatures, as shown in **Figure 7**, at λ and $n = 0$, the values of ε_∞ and ω_p are listed in **Table 1**.

3.4.3.2. The Second Procedure

Determination of the dielectric constant could be defined using the dispersion relation of the incident photon. The refractive index was also fitted using a function for extrapolation towards shorter wavelength. The Moss model [32], which stated that: "the free carriers contribution to dispersion are relatively small". This means that data corresponding to the wavelength range lying below the absorption edge of the material has to be used [33]. The properties of the investigated NiO could be treated as a single oscillator at wavelength λ_o at high frequency. The following equation which calculates the high frequency dielectric constant $\varepsilon_{\infty(2)}$ is:

$$n^2 - 1 = \frac{S_o \lambda_o^2}{1 - (\lambda_o / \lambda)^2} \quad (7)$$

where S_o is the average oscillator strength and λ_o an average oscillator wavelength. Equation (7) can be written in the following former:

$$\frac{n_\infty^2 - 1}{n^2 - 1} = 1 - \left(\frac{\lambda_o}{\lambda}\right)^2 \quad (8)$$

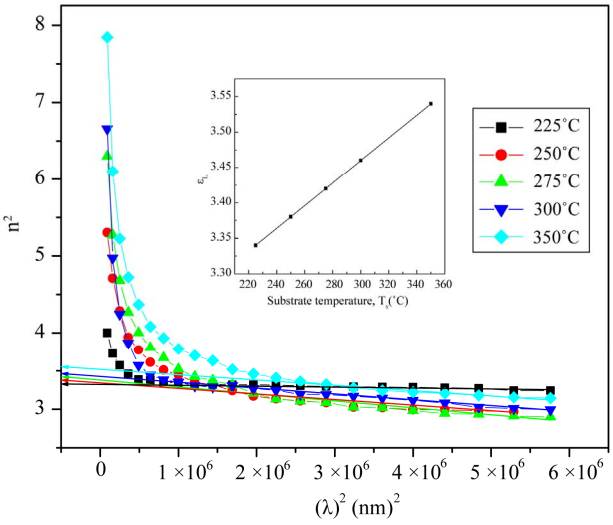

Figure 7. The relation between n^2 and λ^2 for NiO films.

Table 1. Dispersion parameters of NiO thin film prepared at different substrate temperature.

Ts (°C)	ε_L		N/m^* ($cm^{-3} \cdot g^{-1}$) ($\pm 3 \times 10^{-2}$)	λ_o (nm) (± 2)	S_o $(m)^{-2}$ ($\pm 4 \times 10^{-4}$)	ω_p (Hz) ($\pm 4 \times 10^{-3}$)	E_d (eV)	E_o (eV)	E_g (eV)	E_o/E_g	M_{-1}	M_{-3}
	$\varepsilon_{\infty(1)}$ ($\pm 4 \times 10^{-3}$)	$\varepsilon_{\infty(2)}$ ($\pm 6 \times 10^{-3}$)										
225	3.34	3.35	6.25×10^{40}	172	3.4×10^{14}	9.9×10^{8}	17.7	7.50	3.83	1.95	2.36	0.047
250	3.38	3.72	2.54×10^{41}	205	3.03×10^{14}	4.03×10^{9}	18. 5	6.95	3.66	1.89	2.66	0.055
275	3.42	3.93	3.11×10^{41}	222	2.92×10^{14}	4.94×10^{9}	19.0	6.43	3.46	1.85	2.95	0.071
300	3.46	4.22	3.27×10^{41}	232	3.05×10^{14}	5.20×10^{9}	19.2	6.1	3.30	1.85	3.14	0.084
350	3.54	4.34	5.49×10^{41}	245	2.96×10^{14}	8.72×10^{9}	19.4	5.74	3.17	1.81	3.38	0.102

where n_∞ is the refractive index at infinite wavelength. **Table 1** shows the values of λ_o and S_o values were obtained from slope and intercept of $(n^2-1)^{-1}$ versus λ^{-2} curves at different substrate temperatures. The intersection with $(n^2-1)^{-1}$ axis is $(n_\infty^2-1)^{-1}$ and hence, n_∞^2 at λ_o equal to ε_∞. **Figure 8** shows the variation between $(n^2-1)^{-1}$ and λ^{-2} at different substrate temperatures from 225˚C to 350˚C. In addition, the values of the high frequency dielectric constant $\varepsilon_{\infty(2)}$ increased with an increasing in the substrate temperature. The values of $\varepsilon_{\infty(1)}$ and $\varepsilon_{\infty(2)}$ are shown in insert graph and tabulated in **Table 1**. The values of $\varepsilon_{\infty(1)}$ and $\varepsilon_{\infty(2)}$ are closed with each other and small difference between them may be due to the lattice vibrations and bounded carriers in an empty lattice which are in the transparent region [34,35]. The difference between $\varepsilon_{\infty(1)}$ and $\varepsilon_{\infty(2)}$ decreased with increasing substrate temperature. This means that the lattice vibration and bounded currieries decreased with increasing the of substrate temperature.

Moreover, the values of average oscillator strength (S_o) were calculated from **Figure 8**. These values are in a good agreement with that obtained by Assim for TiO films [33], by Abdel-Aziz *et al.* for $GeSe_{(9-x)}Tl_x$ thin-film [36] and also, by Caglar *et al.* for sulfonated poly-aniline film (SPAN) [34]. Unfortunately, there are no data about high frequency dielectric constant of NiO thin films were found to compare.

3.4.4. Dispersion Energy Parameters of NiO Thin Films

The dispersion energy plays an important role in the research for optical materials because it is a significant factor in optical communication and in designing devices for spectral dispersion. The dispersion of refractive index in NiO films was analyzed using the concept of the single oscillator and can be expressed by Wemple and Di-Domenico relationship [35]:

$$n^2-1=\frac{E_dE_o}{\left[E_o^2-E^2\right]} \tag{9}$$

where E, E_o and E_d are the photon energy, the oscillator energy and the dispersion energy, respectively. The parameter E_d, which is the measure of the intensity of the inter-band optical transition, does not depend significantly on the band gap. A plot of $(n^2-1)^{-1}$ versus E^2 of NiO deposited films for different substrate temperatures as shown in **Figure 9**. It is clear that, the effect of substrate temperature on the refractive index and semiconductor dispersion profiles were exhibited a linear displacement in the shape of the dispersion profile with decreasing refractive index. The refractive index declines towards long wavelengths. This is due to the influence of lattice absorption. The values of E_d and E_o were obtained

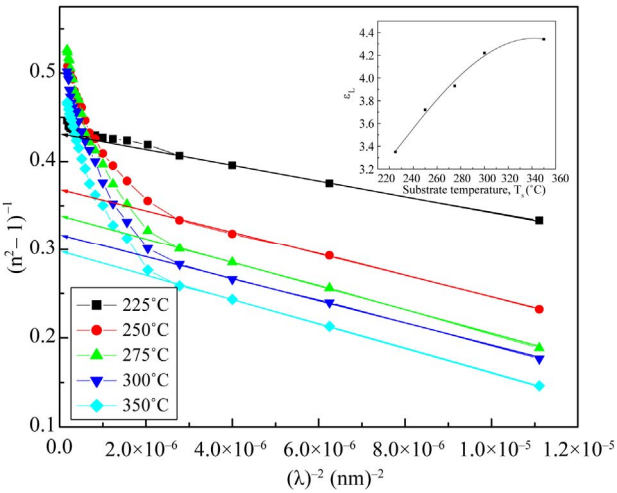

Figure 8. The $(n^2–1)^{-1}$ as a function of reciprocal function of square wavelength for NiO films at different substrate temperature.

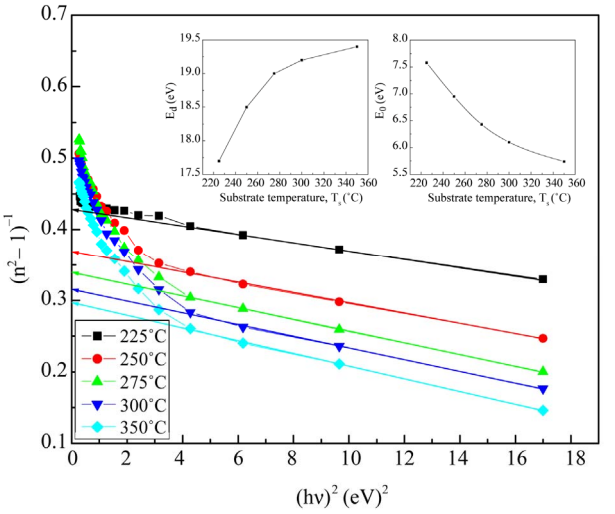

Figure 9. The $(n^2–1)^{-1}$ as a function of reciprocal function of square photon energy for NiO films at different substrate temperature.

from the slope and the intercept, respectively, resulting from the extrapolation of the lines. The individual errors in the calculated E_o and E_d should be significantly small to make the proposed method significant. The values of the standard deviation of the parameters E_o and E_d presented in **Table 1** were calculated by the fitting procedure. The variation of E_o and E_d with different substrate temperatures are shown in **Figure 9**. The values of E_o was found to be decreased with increasing the substrate temperature, while the values of E_d increased with increasing the substrate temperature. This could be attributed to the increase in the number of scattering center due to the dissolving of iridium atoms in the film matrix. The relation between single oscillator energy E_o and en-

ergy gap E_g^d was given by relation of Tanaka [37] as $E_o \approx 2E_g^d$. The average ratio E_o / E_g^d for NiO thin films at different substrate temperatures is calculated as 1.87, which shows an agreement with this relation. A simple connection between the single-oscillator parameters of E_o and E_d and the imaginary part of the dielectric constant, $\varepsilon_{\infty(2)}$, spectrum can be expressed in terms of moments of the $\varepsilon_{\infty(2)}$ as follows [34]:

$$E_o^2 = \frac{M_{-1}}{M_{-3}} \quad \text{and} \quad E_d^2 = \frac{M_{-1}^3}{M_{-3}} \tag{10}$$

The oscillator energy E_o, which was independent of the scale of ε_2 is consequently an ''average'' energy gap, whereas E_d depends on the scale of ε_2 and thus serves as an inter band strength parameter. Since the M_{-1} and M_{-3} moments are involved in computation of E_o and E_d and the values of M_{-1} and M_{-3} are listed in **Table 1**.

4. Conclusions

1) Nickel oxide thin films are prepared by spray pyrolysis technique (SPT) using nickel acetate tetrahydrate solutions onto glass substrates at different temperatures ranged from 225˚C to 350˚C.

2) XRD analyses show that an amorphous films have been obtained at low T_s = 225˚C, while at higher $T_s \geq$ 275˚C a cubic single phase structure of NiO film is formed and the films show prefential growth along the [111] direction.

3) AFM shows relatively smooth surface with 45 nm thick. A grain size analysis of the thicker NiO film gives a mean grain size area of 3.9 μm^2.

4) The refractive index for the prepared films depends on the substrate temperature and film thickness. The higher value of the refractive index at very low temperature at $\lambda > 400$ nm was observed in all samples.

5) The values of $\varepsilon_{\infty(1)}$ and $\varepsilon_{\infty(2)}$, which determined by two different procedures are increased with increasing T_s, while the values of E_o decrease with increasing T_s.

5. References

[1] D. Adler and J. J. Feinleib, "Electrical and Optical Properties of. Narrow-Band Materials," *Physical Review B*, Vol. 2, No. 8, 1970, pp. 3112-3134. doi:10.1103/PhysRevB.2.3112

[2] M. Zöllner, S. Kipp, and K. D. Becker, "Reactive Processes of Nickel Oxide on Oxidic Substrates as Observed by Scanning Force Microscopy," *Crystal Research and Technology*, Vol. 35, No. 3, 2000, pp. 299-305. doi:10.1002/1521-4079(200003)35:3<299::AID-CRAT299>3.0.CO;2-I

[3] E. J. M. O'Sullivan and E. J. Calvo, "Reactions at Metal Oxide Electrodes Comprehensive Chemical Kinetics" Elsevier, New York, 1987.

[4] C. M. Lambert and G. Nazri, P. C. Yu, "Spectroscopic and Electrochemical Studies of Electrochromic Hydrated Nickel Oxide Films," *Solar Energy Materials*, Vol. 16, 1987, pp. 1-17. doi:10.1016/0165-1633(87)90003-7

[5] N. Shaigan, D.G. Ivey and W. Chen, "Metal-Oxide Scale Interfacial Imperfections and Performance of Stainless Steels Utilized as Interconnects in Solid Oxide Fuel Cells," *Journal of The Electrochemical Society*, Vol. 156, No. 6, 2009, pp. B765-B770. doi:10.1149/1.3116252

[6] K.K. Purushothaman and G. Muralidharan, "Nanostructured NiO Based All Solid State Electrochromic Device," *Journal of Sol-Gel Science and Technology*, Vol. 46, 2008, pp. 190-197. doi:10.1007/s10971-007-1657-0

[7] R. Cerc Korosec, P. Bukovec, B. Pihlar, A. Surca Vuk, B. Orel and G.Drazic," Preparation and Structural Investigations of Electrochromic Nanosized NiOx Films Made via the Sol-Gel Route," *Solid State Ionics*, Vol. 165, No. 1-4, 2003, pp. 191-200. doi:10.1016/j.ssi.2003.08.032

[8] B. Sasi and K. G. Gopalchandran, "Nanostructured Mesoporous Nickel Oxide Thin Films," *Nanotechnology*, Vol. 18, 2007, pp. 115613-115617.

[9] H. Kamel, E. K. Elmaghraby, S. A. Ali and K. Abdel-Hady," The Electrochromic Behavior of Nickel Oxide Films Sprayed at Different Preparative Conditions," *Thin Solid Films*, Vol. 483, No. 1-2, 2005, pp. 330-339. doi:10.1016/j.tsf.2004.12.022

[10] A. Mendoza-Galván, M. A. Vidales-Hurtado and A. M. López-Beltrán, "Comparison of the Optical and Structural Properties of Nickel Oxide-Based Thin Films Obtained by Chemical Bath and Sputtering," *Thin Solid Films*, Vol. 517, No. 10, 2009, pp. 3115-3120. doi:10.1016/j.tsf.2008.11.094

[11] I. Valyukh, S. Green, H. Arwin, G. A. Niklasson, E. Wäckelgård and C. G. Granqvist, "Spectroscopic Ellipsometry Characterization of Electrochromic Tungsten Oxide and Nickel Oxide Thin Films Made by Sputter Deposition," *Solar Energy Materials & Solar Cells*, Vol. 94, 2010, pp. 724-733. doi:10.1016/j.solmat.2009.12.011

[12] M.A. Vidales-Hurtado and A. Mendoza-Galv´an, "Optical and Structural Characterization of Nickel Oxide-Based Thin Films Obtained by Chemical Bath Deposition," *Materials Chemistry and Physics*, Vol. 107, No. 1, 2008, pp. 33-38. doi:10.1016/j.matchemphys.2007.06.036

[13] E. Ozkan Zayim, I. Turhan, F.Z. Tepehan and N. Ozer, "Sol-Gel Deposited Nickel Oxide Films for Electrochromic Applications," *Solar Energy Materials & Solar Cells*, Vol. 92, 2008, pp. 164-196. doi:10.1016/j.solmat.2007.03.034

[14] J. D. Desai, S.-K. Min, K.-D. Jung and O.-S. Joo, "Spray pyrolytic Synthesis of Large Area NiOx Thin Films from Aqueous Nickel Acetate Solutions," *Applied Surface Science*, Vol. 253, 2006, pp. 1781-1788. doi:10.1016/j.apsusc.2006.03.009

[15] R. Romero, F. Martin, J.R. Ramos-Barrado and D. Leinen, "Synthesis and Characterization of Nanostructured Nickel Oxide Thin Films Prepared with Chemical Spray Pyroly-

sis," *Thin Solid Films*, Vol. 518, No. 16, 2010, pp. 4499-4502. doi:10.1016/j.tsf.2009.12.016

[16] A. Richter and R. Ries, "Surface Growth Modes Analysed with Modern Microscopic and Computing Techniques," *European Journal of Physics*, Vol. 17, 1996, pp. 311-318. doi:10.1088/0143-0807/17/6/002

[17] H. Kamal, E. K. Elmaghraby, S. A. Aly and K. Abdel-Hady, "Characterization of Nickel Oxide Films Deposited at Different Substrate Temperatures Using Spray Pyrolysis," *Journal of Crystal Growth*, Vol. 262, No. 1-4, 2004, pp. 424-434. doi:10.1016/j.jcrysgro.2003.10.090

[18] A. A. Al-Ghamdi, W. E. Mahmoud, S. J. Yaghmour and F. M. Al-Marzouki, "Structure and Optical Properties of Nanocrystalline NiO Thin Film Synthesized by Sol-Gel Spin-Coating Method," *Journal of Alloys and Compounds*, Vol. 486, No. 1-2, 2009, pp. 9-13. doi:10.1016/j.jallcom.2009.06.139

[19] S. A. Mahmoud, A. Akl, H. Kamal and K. Abdel-Hady, "Opto-Structural, Electrical and Electrochromic Properties of Crystalline Nickel Oxide Thin Films Prepared by Spray Pyrolysis," *Physica B*, Vol. 311, No. 3-4, 2002, pp. 366-375. doi:10.1016/S0921-4526(01)01024-9

[20] C. Navone, J.P. Pereira-Ramos, R. Baddour-Hadjean and R. Salot, "Electrochemical and Structural Properties of V_2O_5 Thin Films Prepared by DC Sputtering," *Journal of Power Sources*, Vol. 146, 2005,pp. 327-330. doi:10.1016/j.jpowsour.2005.03.024

[21] J. Tauc, "Amorphous and Liquid Semiconductors," Plenum Press, New York, 1974.

[22] S. A. Mahmoud, A. A. Akl, and S. M. Al-Shomar, "Preparative Parameters-Dependent Optical Properties of Spray Deposited Iridium Oxide Thin Films," *Physica B*, Vol. 404, No. 16, 2009, pp. 2151-2158. doi:10.1016/j.physb.2009.04.003

[23] C. Shi, G. Wang, N. Zhao, X. Du and J. Li, " NiO Nanotubes Assembled in Pores of Porous Anodic Alumina and Their Optical Absorption Properties," *Chemical Physics Letters*, Vol. 454, 2008, pp. 75-79. doi:10.1016/j.cplett.2008.01.069

[24] S. A. Mahmoud, "Structural and Physical Properties of Sprayed SnO_2 Films Doped with Flurine," *Egyptian Journal of Solids*, Vol. 19, 1996, pp. 221-228.

[25] J. N. Zemel, J. D. Jensen and R. B. Schoolar, "Electrical and Optical Properties of Epitaxial Films of PbS, PbSe, PbTe, and SnTe," *Physical Review A*, Vol. 140, 1965, pp. 330-335. doi:10.1103/PhysRev.140.A330

[26] M. B. El-Den and M. M. El-Nahass, "Optical Properties of $AsSe_{1.5-x}T_x$ Glassy System," *Optics & Laser Technology*, Vol. 35, No. 5, 2003, pp. 335-340. doi:10.1016/S0030-3992(03)00008-2

[27] M. G. Hutchins, O. Abu-Alkhair, M. M. El-Nahass and K. Abdel-Hady, "Structural and Optical Characterisation of Thermally Evaporated Tungsten Trioxide (WO_3) Thin Films," *Materials Chemistry and Physics*, Vol. 98, No. 2-3, 2006, pp. 401-405. doi:10.1016/j.matchemphys.2005.09.052

[28] M. M. El-Nahass, A. M. Farag, K. F. Abd El-Rahman and A. A. A. Darwish, "Dispersion Studies and Electronic Transitions in Nickel Phthalocyanine Thin Films," *Optics & Laser Technology*, Vol. 37, No. 7, 2005, pp. 513-523. doi:10.1016/j.optlastec.2004.08.016

[29] M. M. El-Nahass, M. M. Sallam and A. H. S. Abdel-Wahab, "Optical and Photoelectric Properties of $TlInS_2$ Layered Single Crystals," *Current Applied Physics*, Vol. 9, 2009, pp. 311-316. doi:10.1016/j.cap.2008.02.011

[30] M. Baleva, E. Goranova, V. Darakchieva, S. Kossionides, M. Kokkosis and P. Jordanov, "Influence of Grain Size on the Optical Conductivity of β-$FeSi_2$ Layers," *Vacuum*, Vol. 69, No. 1, 2002, pp. 425-429. doi:10.1016/S0042-207X(02)00369-X

[31] V. Darakchieva, M. Baleva, M. Surtchey and E. Goranova, "Structural and Optical Analysis of β-$FeSi_2$ Thin Layers Prepared by Ion-Beam Synthesis and Solid-State Reaction," *Physical Review B*, Vol. 62, 2000, pp. 13057-13059. doi:10.1103/PhysRevB.62.13057

[32] T. S. Moss, "Optical Properties of Semiconductors," Butterworth's Scientific Publication LTD., London, 1959.

[33] E. M. Assim, "Optical Constants of $TiO_{1.7}$ Thin Films Deposited by Electron Beam Gun," *Journal of Alloys Compounds*, Vol. 463, No. 1, 2008, pp. 55-61. doi:10.1016/j.jallcom.2007.09.034

[34] M. Caglar, S. Ilican, Y. Calgan, Y. Sahin, F. Yakuphanoglu and D. Hur, "A Spectro Electrochemical Study on Single-Oscillator Model and Optical Constants of Sulfonated Polyaniline Film," *Spectrochimica Acta A*, Vol. 71, No. 2, 2008, pp. 621-627. doi:10.1016/j.saa.2008.01.022

[35] S. H. Wemple and M. DiDomenco, "Behavior of the Electronic Dielectric Constant in Covalent and Ionic Materials," *Physical Review B*, Vol. 3, 1971, pp. 1338-1342. doi:10.1103/PhysRevB.3.1338

[36] M. M. Abdel-Aziz, E. G. El-Metwally, M. Fadel, H. H. Labib and M. A. Afifi," Optical Properties of Amorphous Ge—Se—Tl System Films," *Thin Solid Films*, Vol. 386, No. 1, 2000, pp. 99-104. doi:10.1016/S0040-6090(01)00765-9

[37] K. Tanaka, "Optical Properties and Photoinduced Changes in Amorphous As-S Films," *Thin Solid Films*, Vol. 66, No. 3, 1980, pp. 271-279. doi:10.1016/0040-6090(80)90381-8

